Atmos. Chem. Phys. Discuss., doi:10.5194/acp-2016-1022, 2016
Manuscript under review for journal Atmos. Chem. Phys.
Published: 19 December 2016


Atmospheric Chemistry and Physics Discussions

# Contribution of Surface Solar Radiation and Precipitation to Spatiotemporal Patterns of Surface and Air Temperature Warming in China from 1960 to 2003

Jizeng Du[1,2], Kaicun Wang[1,2*], Jiankai Wang[3], Qian Ma[1,2]

[1]College of Global Change and Earth System Science, Beijing Normal University, Beijing, 100875, China

[2]Joint Center for Global Change Studies, Beijing 100875, China

[3]Chinese Meteorological Administration, Beijing, 100081, China

**Corresponding Author**: Kaicun Wang, College of Global Change and Earth System Science, Beijing Normal University. Email: kcwang@bnu.edu.cn; Tel: +086 10-58803143; Fax: +086 10-58800059.

Atmos. Chem. Phys. Discuss., doi:10.5194/acp-2016-1022, 2016
Manuscript under review for journal Atmos. Chem. Phys.
Published: 19 December 2016


Atmospheric Chemistry and Physics Discussions


## Abstract

Although the global warming has been successfully attributed to the elevated atmospheric greenhouses gases, the reasons for spatiotemporal patterns the warming rates are still under debate. In this paper, we report surface and air warming based on observations collected at 1977 stations in China from 1960 to 2003. Our results show that the warming of daily maximum surface ($T_{s\text{-}max}$) and air ($T_{a\text{-}max}$) temperatures showed a significant spatial pattern, stronger in the northwest China and weaker in South China and the North China Plain. These warming spatial patterns are attributed to surface shortwave solar radiation (SSR) and precipitation, the key parameters of surface energy budget. During the study period, SSR decreased by $-1.50$ W m$^{-2}$ 10yr$^{-1}$ in China and caused the trends of Ts-max and Ta-max decreased by 0.139 and 0.053 °C 10yr$^{-1}$, respectively. More importantly, South China and the North China Plain had an extremely higher dimming rates than other regions. The spatial contrasts of trends of $T_{s\text{-}max}$ and $T_{a\text{-}max}$ in China are significantly reduced after adjusting for the impact of SSR and precipitation. For example, the difference in warming rates between North China Plain and Loess Plateau reduce by 97.8% and 68.3% for Ts-max and Ta-max respectively. After adjusting for the impact of SSR and precipitation, the seasonal contrast of $T_{s\text{-}max}$ and $T_{a\text{-}max}$ decreased by 45.0% and 17.2%, and the daily contrast of warming rates of surface and air temperature decreased by 33.0% and 29.1% over China.

Atmos. Chem. Phys. Discuss., doi:10.5194/acp-2016-1022, 2016
Manuscript under review for journal Atmos. Chem. Phys.
Published: 19 December 2016


Atmospheric Chemistry and Physics Discussions

This study shows an essential role of land energy budget in determining regional warming.

## 1. Introduction

With the rapid development of observational data and the simulation abilities of climate models, global warming has been regarded as undeniable (Hartmann et al., 2013). The increase in anthropogenic greenhouse gases and other anthropogenic impacts are believed to be the primary cause of global warming. However, there are significant spatial and temporal heterogeneities in climate warming, i.e., faster warming rates in semiarid regions and a “warming hole” in the central United States (Boyles and Raman, 2003; Huang et al., 2012), which represents a major barrier to the reliable detection and attribution of global warming (Tebaldi et al., 2005; Mahlstein and Knutti, 2010). Furthermore, the uncertainties in model simulations generally increase from the global to the regional scale because of uncertainty in regional climatic responses to global change (Hingray et al., 2007; Mariotti et al., 2011). Therefore, it is crucial to research not only the spatial and temporal patterns of regional climate changes but also regional climatic response mechanisms to global change. This approach can improve confidence in the detection and attribution of global climate change and prediction of future regional climate change.

Atmos. Chem. Phys. Discuss., doi:10.5194/acp-2016-1022, 2016
Manuscript under review for journal Atmos. Chem. Phys.
Published: 19 December 2016


Atmospheric Chemistry and Physics Discussions

52 The spatial heterogeneity of climate warming can be attributed to local climate
53 factors and anthropogenic factors (Karl et al., 1991). For the former, local determining
54 factors such as cloud amounts and precipitation can significantly influence regional
55 warming speeds (Hegerl and Zwiers, 2007; Lauritsen and Rogers, 2012). Those spatial
56 heterogeneities in climate-factor trends make important contributions to various
57 changes in the land-surface energy balance. Existing studies have indicated that an
58 increase in clouds can diminish downward shortwave solar radiation to the land surface,
59 thus reducing the daytime temperature (Dai et al., 1997; Zhou et al., 2010; Taylor et al.,
60 2011) while potentially increasing nighttime temperatures by intercepting outgoing
61 longwave radiation (Shen et al., 2014; Campbell and VonderHaar, 1997).

62 Precipitation can alter the proportion of surface absorbed energy partitioned into
63 sensible heat flux and latent heat flux and therefore has an inevitable impact on both
64 land-surface and near-surface air temperatures (Wang and Dickinson, 2012; Wang and
65 Zhou, 2015). In addition, precipitation plays a key role in the soil thermal inertia and
66 surface vegetation, causing important feedback to regional and global warming (Wang
67 and Dickinson, 2012; Seneviratne et al., 2010; Ait-Mesbah et al., 2015; Shen et al.,
68 2015).

69 In addition to local climate factors, anthropogenic emissions of aerosols have a

Atmos. Chem. Phys. Discuss., doi:10.5194/acp-2016-1022, 2016
Manuscript under review for journal Atmos. Chem. Phys.
Published: 19 December 2016




significant effect on the regional climate system. Studies indicated that improving air quality in recent decades has led to brightening over North America and Europe (Wild, 2012; Vautard et al., 2009), whereas surface shortwave solar radiation (SSR) has declined in East Asia and India with increasing air pollution (Xia, 2010; Menon et al., 2002; Wang et al., 2012; Wang et al., 2015a). Consequently, the variation in SSR may have an impact on both local and global climate change (Wild et al., 2007; Wang and Dickinson, 2013b).

Land cover change can also alter the energy exchange between the land surface and the atmosphere; moreover, it has the potential to impact regional climate (Falge et al., 2005; Bounoua et al., 1999; Zhou et al., 2004). Previous studies have suggested that urbanization and other land-use changes contribute to promoting the warming effect caused by greenhouse gases (Kalnay and Cai, 2003; Lim et al., 2005; Chen et al., 2015). Overall, the impacts of these factors on climate change may be very important on the regional scale, leading to a marked spatial difference in regional climate change, whereas they are usually omitted from the detection and attribution of climate change on the global scale (Karoly and Stott, 2006).

China has a vast territory and abundant types of climactic zones stretching from tropic to cold temperate, with a special alpine climate over the Tibet Plateau. In addition,

Atmos. Chem. Phys. Discuss., doi:10.5194/acp-2016-1022, 2016
Manuscript under review for journal Atmos. Chem. Phys.
Published: 19 December 2016


Atmospheric Chemistry and Physics Discussions

dramatic economic development and explosive population growth in recent decades has caused significant land cover change and serious air pollution, including frequent haze events (Yin et al., 2016; Cheng et al., 2014; Wang et al., 2016). The climatic diversity and intensive human activity in this region will likely lead to a unique response to global warming with obvious spatial differences in climate change.

Karl et al. (1991) had analyzed the observational records for the period 1951-1989, finding that China's temperature warming trends were faster than those of the United States but slower than those of the former Soviet Union. Several studies had revealed that the warming rate in Northwest China had been approximately 0.33-0.39 °C $10yr^{-1}$ during the second half of the last century (Li et al., 2012; Zhang et al., 2010), which was significantly higher than the average warming rate over China (0.25 °C $10yr^{-1}$) (Ren et al., 2005) or that on a global scale (0.13 °C $10yr^{-1}$) (Hegerl and Zwiers, 2007). Air temperatures (Ta) over the Tibet Plateau have increased by 0.44 °C $10yr^{-1}$ over the last 30 years (Duan and Xiao, 2015), which was considerably faster than the overall warming rate in the Northern Hemisphere (0.23 °C $10yr^{-1}$) and worldwide (0.16 °C $10yr^{-1}$) (Hartmann et al., 2013). Understanding the characteristics and mechanisms of regional climate change is critical to advancing the knowledge and predication of future climate change.

Atmos. Chem. Phys. Discuss., doi:10.5194/acp-2016-1022, 2016
Manuscript under review for journal Atmos. Chem. Phys.
Published: 19 December 2016


Atmospheric Chemistry and Physics Discussions

106 Ta is a common metric for judging climate change on the global or regional scales.
107 However, land surface temperature (Ts) is beginning to play an increasingly important
108 role in climate change research because it has the distinct advantage of being directly
109 related to the land surface energy budget. Previously, $T_s$ values used in regional climate
110 research are primarily derived from satellite retrievals or reanalysis datasets (Weng et
111 al., 2004; Peng et al., 2014), both of which have good global coverage but questionable
112 accuracy and integrity. Furthermore, satellite-derived $T_s$ values are only available under
113 clear sky conditions, limiting their application to climate change studies.

114 In China, $T_s$ has been measured as a conventional meteorological observation item
115 by nearly all weather stations, as is $T_a$. This study found that observations of $T_s$ have a
116 good relationship with $T_a$ in terms of spatial-temporal patterns and can equally
117 accurately reflect the characteristics of climate change. More importantly, $T_s$ is more
118 sensitive to the local land surface energy budget, particularly surface solar radiation
119 (SSR) and precipitation.

120 From the perspective of energy, both SSR and precipitation are key factors
121 controlling the land surface energy budget; therefore, their changes most likely cause
122 regional differences in the warming rate of Ta (Wild, 2012; Manara et al., 2015;
123 Hartmann et al., 1986). For the first time, this study analyzed the relationship between

Atmos. Chem. Phys. Discuss., doi:10.5194/acp-2016-1022, 2016
Manuscript under review for journal Atmos. Chem. Phys.
Published: 19 December 2016




SSR (and precipitation) and $T_a$ or $T_s$ in terms of their spatial–temporal patterns and further quantified the impact of the variations of SSR and precipitation on $T_a$ and $T_s$ in China for the period of 1960–2003.

This paper is organized as follows: Section 2 introduces the data and method used in the study. Section 3 includes three parts: the first part describes the spatial and temporal pattern of climate warming over China; the second part analyzes the impact of the variation in SSR and precipitation on $T_a$ and $T_s$; and the third part illustrates the spatial and temporal pattern of the warming trend of $T_a$ and $T_s$ after adjusting for the impact of SSR and precipitation. The adjustment removed impact of land-atmosphere interaction on the warming, leaving impact of large scale warming caused by the elevated atmospheric greenhouse gases substantially. Our results show that adjustment substantially reduced the spatial contrast of warming trends of Ta and Ts in China, which is agree with the expectation of global warming. A summary and discussion are presented in Section 4.

## 2. Data and method

### 2.1. Data

The meteorological observational data used in this study are recently released daily

Atmos. Chem. Phys. Discuss., doi:10.5194/acp-2016-1022, 2016
Manuscript under review for journal Atmos. Chem. Phys.
Published: 19 December 2016


Atmospheric Chemistry and Physics Discussions

meteorological datasets, including the China National Stations' Fundamental Elements Datasets V3.0 (CNSFED V3.0), which can be downloaded from the China's National Meteorological Information Center (http://data.cma.gov.cn/data) (Cao et al., 2016). This dataset includes $T_s$, $T_a$, the barometric pressure, relative humidity, and sunshine duration. All of the observational records of the climate variables include quality control and homogenization of the processes of data acquisition and compilation.

Figure 1 shows that the number of stations used in this study (1977 selected stations from a total of 2479 stations) is abundant and significantly greater than in previous studies (i.e., 57-852 stations) (Kukla and Karl, 1993; Shen and Varis, 2001; Liu et al., 2004; Li et al., 2015); therefore, the observational data have better spatial coverage and higher confidence of detecting regional climate change (Fig. 1). Our study is the first to use the observations of $T_s$ for research into regional climate change.

Observations of $T_s$ at weather stations are different from data retrieved via other approaches, such as satellite data and reanalysis. All of the observational fields of $T_s$ are 4 m × 2 m square bare land plots in a weather station. The surface of the observational field must be kept loose, grassless, flat, and at the same level as the ground of the weather station. Three thermometers are placed on the surface of the observational field, including a surface thermometer, a surface maximum thermometer,

Atmos. Chem. Phys. Discuss., doi:10.5194/acp-2016-1022, 2016
Manuscript under review for journal Atmos. Chem. Phys.
Published: 19 December 2016


Atmospheric Chemistry and Physics Discussions

and a surface minimum thermometer. The thermometers are deposited on the surface of the observational field horizontally: half of each thermometer is embedded in the soil and the other half is exposed to the air. When the observational field is covered by snow, the thermometers are removed from the snow and placed on the snow surface. In addition, the exposed parts of the thermometers must be kept clean from dust and dew.

To verify the reliability of the $T_s$ observational records, we analyzed the relationship between $T_a$ and $T_s$ in the observed records for 1960–2003. As shown in Figures. S1, the mean Pearson Correlation Coefficients between $T_{s\text{-}max}$ and $T_{a\text{-}max}$ calculated from the monthly anomalies were 0.775, 0.843, and 0.806 for the annual, warm, and cold seasonal scales, respectively, and were statistically significant (99% confidence) for all stations. The mean correlation coefficients between $T_{s\text{-}min}$ and $T_{a\text{-}min}$ were 0.861, 0.842, and 0.865 for the annual, warm, and cold seasonal scales, respectively, and were statistically significant (99% confidence) for all stations. The high correlation between $T_a$ and $T_s$ indicates that the observations of $T_s$ are reliable for detecting climate change.

SSR is the most fundamental energy resource for $T_s$ and $T_a$. Most previous studies had used the observed SSR to analyze the relationship between the variation in SSR and $T_a$ over Mainland China. However, sites for SSR observation were far less

Atmos. Chem. Phys. Discuss., doi:10.5194/acp-2016-1022, 2016
Manuscript under review for journal Atmos. Chem. Phys.
Published: 19 December 2016


Atmospheric Chemistry and Physics Discussions

numerous than those for other climatic variables, i.e., only 85 sites were used for SSR observation in Liu et al. (2004); 90 sites were used in Li et al. (2015).

More importantly, it was found that sensitivity drifting of the instruments used for the SSR observations led to a faster dimming rate before 1990 and that instrument replacements from 1990 to 1993 had resulted in a falsely sharp increase in SSR (Wang, 2014; Wang et al., 2015a). The sparse distribution and low quality of SSR observations make it difficult to quantify the variation in SSR and detect its impact on climate change.

We therefore used sunshine duration-derived SSR in this study, which is based on an effective hybrid model developed by Yang et al. (2006). This model has subsequently been improved (Wang et al., 2015a; Wang, 2014) and has proved to be performed well in regional and global applications (Tang et al., 2011; Wang et al., 2012). Sunshine duration-derived solar radiation not only can accurately reflect the impact of clouds and aerosols on the SSR but also can more exactly reveal long-term SSR trends (Wang et al., 2015a; Wang, 2014). Sunshine duration has a better correlation with the satellite-derived SSR, reanalysis, and climate model simulations of SSR than the observed SSR in China (Wang et al., 2015a).

There are 2,474 meteorological stations reporting data; however, the lengths of the effective observation records for the stations are different. In addition, only a small

Atmos. Chem. Phys. Discuss., doi:10.5194/acp-2016-1022, 2016
Manuscript under review for journal Atmos. Chem. Phys.
Published: 19 December 2016




number of stations existed prior to 1960 and the observational records of $T_s$ at many stations became significantly abnormal after 2003 because of automation. Therefore, in our analysis, we selected 1,977 meteorological stations (see Fig. 1) that the valid data of observation record must be longer than 30 years during the period of 43 years between 1960 and 2003.

The monthly anomaly relative to the 1961-1990 climatology was calculated based on a monthly mean value of the daily observation value, and if a month has more than 7 daily missing values, it was classified as a missing value (Sun et al., 2016; Li et al., 2015). The annual anomalies are the average of the monthly anomalies for the entire year. The anomalies in the warm seasons are the averages of the monthly anomalies from May to October, and the anomalies in the cold seasons are the averages of the monthly anomalies from November to the next April.

### 2.2 Method

As shown in Fig. 1, the spatial distribution of the weather stations over Mainland China is extraordinarily asymmetric and the density of weather stations in East China is far greater than in West China. We used the area-weight average method to reduce these biases when calculating the national mean. First, we divided the study region into 1° × 1° grids (see Fig. S2); there are 953 grids over China. Second, we assigned all

Atmos. Chem. Phys. Discuss., doi:10.5194/acp-2016-1022, 2016
Manuscript under review for journal Atmos. Chem. Phys.
Published: 19 December 2016




selected stations to the grids; there are 627 grids with stations, accounting for 65.79% of the total. Finally, the grid box value is taken to be the average of all of the stations on the grid, and the national mean is the area-weight average of all of the effective grids (Jones and Moberg, 2003).

The linear trends reported in this study were calculated by a linear regression based on the least square method. Based on the anomalies of grids, there are two common ways to calculate the national mean trends of the variables in China. The first method (Method I) calculates the national mean monthly anomalies by taking the area-weight of every grid first and then calculates the national mean trend based on the time series of the national average anomalies. The second method (Method II) calculates the trend at every grid first and then the national mean trend over China is the area-weighted average value of the trends on all of the grids. In our study, we calculated the national mean trends of the temperatures using both methods as both methods are widely used in the existing studies (Gettelman and Fu, 2008). Same results are derived from those two methods if time series of all grids is integral and have no missing data (Zhou et al., 2009). However, as noted, we selected 1,977 stations (see Fig. 1) that the valid data of observation records are longer than 30 years during the period 1960-2003, which is a reasonable compromise between the integrity of the observation records and the spatial coverage. The missing data in the time series for some grids results in a little difference

Atmos. Chem. Phys. Discuss., doi:10.5194/acp-2016-1022, 2016
Manuscript under review for journal Atmos. Chem. Phys.
Published: 19 December 2016




232 between the results of these two methods. To avoid misunderstanding, the trends
233 derived from Method I was discussed in the main text, but results from two methods
234 were shown in Table 1.

235 In this study, a multiple linear regression (see Eq. (1)) was used to calculate the
236 sensitivity and impact of changes of SSR and precipitation on the temperatures (Roy
237 and Haigh, 2011). This can be expressed as

238 $$z = a \cdot x + b \cdot y + c + \varepsilon \quad (1)$$

239 where **z** represents the monthly anomalies of $T_{s\text{-}max}$, $T_{s\text{-}min}$, $T_{a\text{-}max}$, and $T_{a\text{-}min}$; ***x*** and ***y*** are
240 the monthly anomalies of the SSR and precipitation, respectively; ***a*** and ***b*** are the
241 corresponding sensitivities of the temperatures to SSR and precipitation, respectively;
242 ***c*** is constant term; and $\boldsymbol{\varepsilon}$ indicates the residuals of the equation.

243 To adjust for the impact of SSR and precipitation on temperatures, we took ***x*** as a
244 time series of SSR and ***y*** as a time series of precipitation, while ***a*** and ***b*** are the
245 sensitivities of the climate variables to changes in SSR and precipitation, respectively.
246 The method of adjusting for the impact of SSR and precipitation is expressed as

247 $$T_{adjusted} = T_{raw} - a \cdot x - b \cdot y \quad (2)$$

Atmos. Chem. Phys. Discuss., doi:10.5194/acp-2016-1022, 2016
Manuscript under review for journal Atmos. Chem. Phys.
Published: 19 December 2016




where $T_{adjusted}$ indicates the value of the climate variables after adjusting for the impact of SSR and precipitation and $T_{raw}$ is the value of the climate variables in the raw data.

## 3. Results

### 3.1. Trends of surface temperature and air temperature

#### 3.1.1 The temporal patterns in the variabilities of the temperatures

Figs. 2 and Figs. 3 show the long-term changes in $T_{s\text{-}max}$ and $T_{a\text{-}max}$, $T_{s\text{-}min}$ and $T_{a\text{-}min}$ from 1960 to 2003 respectively. In addition to annual variability (Figs. 2a and Figs. 3a), we analyzed the variabilities of the temperatures in both the warm seasons (May-October) (Figs. 2b and Figs. 3b) and the cold seasons (November to the following April) (Figs. 2c and Figs. 3c). In the annual records, all of the temperatures showed an obvious warming trend over China (Figs. 2a and Figs. 3a). As shown in Table 1, the national mean warming rate for $T_{s\text{-}max}$ was 0.227 °C $10yr^{-1}$ and the rate for $T_{a\text{-}max}$ was 0.167 °C $10yr^{-1}$ from 1960 to 2003. The warming rate of $T_{a\text{-}max}$ based on the 1,977 stations in this paper was a little higher than both that of the global average (0.141 °C $10yr^{-1}$) from 1950 to 2004 (Vose et al., 2005) and that of a previous analysis of China (0.127 °C $10yr^{-1}$) from 1955 to 2000 based on 305 stations (Liu et al., 2004).

The seasonal contrasts of warming of $T_{a\text{-}max}$ and $T_{s\text{-}max}$ are important. $T_{s\text{-}max}$ had an

Atmos. Chem. Phys. Discuss., doi:10.5194/acp-2016-1022, 2016
Manuscript under review for journal Atmos. Chem. Phys.
Published: 19 December 2016


Atmospheric Chemistry and Physics Discussions

265 average rate of 0.172 °C 10yr$^{-1}$ in the warm seasons and 0.354 °C 10yr$^{-1}$ in the cold
266 seasons. For $T_{a\text{-}max}$, it was 0.091 °C 10yr$^{-1}$ and 0.294 °C 10yr$^{-1}$ in the warm and cold
267 seasons, respectively. The increases in $T_{s\text{-}max}$ and $T_{a\text{-}max}$ in the cold seasons were much
268 larger than those in the warm seasons, which is consistent with previous studies of
269 China and other regions (Shen et al., 2014; Vose et al., 2005; Ren et al., 2005).

270 Similarly, the warming rates of $T_{s\text{-}min}$ and $T_{a\text{-}min}$ in the warm seasons were clearly
271 lower than those in the cold seasons too. As shown in Figs. 3, $T_{s\text{-}min}$ increased by
272 0.315 °C 10yr$^{-1}$ and $T_{a\text{-}min}$ increased by 0.356 °C 10yr$^{-1}$ (see Figs. 3a) from 1960 to
273 2003. The warming trend of $T_{a\text{-}min}$ is generally consistent with earlier studies (Shen et
274 al., 2014; Li et al., 2015; Liu et al., 2004); however, it is considerably larger than that
275 reported for the global average (0.204 °C 10yr$^{-1}$) (Vose et al., 2005). $T_{s\text{-}min}$ increased at
276 a rate of 0.221 °C 10yr$^{-1}$ in the warm seasons and 0.447 °C 10yr$^{-1}$ in the cold seasons
277 from 1960 to 2003. $T_{a\text{-}min}$ increased at rates of 0.245 °C 10yr$^{-1}$ and 0.505 °C 10yr$^{-1}$ in
278 the warm and cold seasons, respectively.

279 On a national average scale, all temperatures increased from 1960 to 2003. The
280 warming rate of $T_{s\text{-}min}$ ($T_{a\text{-}min}$) was significantly faster than that of $T_{s\text{-}max}$ ($T_{a\text{-}max}$) and the
281 warming rates of all temperatures in cold seasons were generally higher than those in
282 warm seasons. These basic characteristics of the temperature changes are consistent

Atmos. Chem. Phys. Discuss., doi:10.5194/acp-2016-1022, 2016
Manuscript under review for journal Atmos. Chem. Phys.
Published: 19 December 2016




283 with previous studies on global or regional scales (Li et al., 2015; Liu et al., 2004;
284 Easterling et al., 1997). For the daily contrast in warming rates, there are still apparent
285 uncertainties in its causes and physical mechanism (Hartmann et al., 2013). Some
286 previous studies hold an opinion that the microclimate (e.g. urban heat island) has a
287 larger impact on minimum temperatures due to the lower and more stable boundary
288 layer at night (Zhou and Ren, 2011; Christy et al., 2009), while many investigators
289 argued that the variabilities of surface solar radiation are the main reason for this daily
290 contrast in warming rates (Sanchez-Lorenzo and Wild, 2012; Makowski et al., 2009).
291 For seasonal contrast in warming rates of temperatures, previous studies attributed that
292 the most precipitation are concentrated in warm season because of monsoonal climate
293 in China. The higher relative humidity in warm seasons will suppress changes of
294 temperatures (Liu et al., 2004; Karl et al., 1993). In this paper, our results had partly
295 explained the causes of those daily or seasonal contrast in warming rates of
296 temperatures.

297 However, there remain slight differences between our results and previous studies
298 with respect to the temperature warming rates, which might have several causes. The
299 number of stations used in our study is much greater than in previous studies, which
300 has led to better spatial coverage and a better representation of our analytical result. In
301 addition, we used the area-weight average method both to reduce the impact of uneven

Atmos. Chem. Phys. Discuss., doi:10.5194/acp-2016-1022, 2016
Manuscript under review for journal Atmos. Chem. Phys.
Published: 19 December 2016




302 station densities and to improve the representation of West China, which has a sparse
303 station distribution (see Fig. 1), when calculating the national mean trend. Previous
304 studies had indicated that the Tibet Plateau and the northwestern arid and semiarid
305 regions were experiencing significantly more rapid warming trends than other regions
306 in China (You et al., 2016), which may lead to our results being slightly higher than
307 those of previous studies. In addition, the study periods of the various studies are not
308 exactly the same. In addition, differences in the method used to calculate the national
309 mean trend also may result in significant differences. As shown in Table 1, the absolute
310 value of difference between Method I and Method II ranges from 0.011 to 0.033 °C
311 $10yr^{-1}$, account for 3.4% to 14.3% of trends (taking the results of Method I as reference).

312 **3.1.2. The spatial patterns in the variabilities for the temperatures**

313 Figs. 4 demonstrates a clear spatial heterogeneity in the warming rates for $T_{s\text{-}max}$
314 and $T_{a\text{-}max}$ over China from 1960-2003. $T_{s\text{-}max}$ and $T_{a\text{-}max}$ increased at high rate and the
315 trends of $T_{s\text{-}max}$ and $T_{a\text{-}max}$ were statistically significant in the Tibet Plateau, and
316 Northwest and Northeast China (see Figs. S3). However, $T_{s\text{-}max}$ and $T_{a\text{-}max}$ had a relative
317 lower warming rate in the North China Plain and South China, and $T_{s\text{-}max}$ even showed
318 cooling trends in the Sichuan Plain, the Yangtze River Delta, and the Pearl River Delta.
319 Lower warming rates of Ta-max in South China and the North China Plain had also

Atmos. Chem. Phys. Discuss., doi:10.5194/acp-2016-1022, 2016
Manuscript under review for journal Atmos. Chem. Phys.
Published: 19 December 2016


Atmospheric Chemistry and Physics Discussions

been reported in multiple previous studies (Liu et al., 2004; Li et al., 2015).

For $T_{s\text{-}max}$ and $T_{a\text{-}max}$, the warming rates of South China and the North China Plain in the warm seasons were considerably lower than those in the cold seasons, resulting in a more obvious spatial heterogeneity in the warm seasons (Figs. 4b and 4h). However, the warming rates of both $T_{s\text{-}max}$ and $T_{a\text{-}max}$ in the Sichuan Basin and the Pearl River Delta were lower in the cold seasons than in the warm seasons. Despite of the spatial and seasonal patterns of $T_{a\text{-}max}$ were clearly similar to those of $T_{s\text{-}max}$. For $T_{a\text{-}max}$, both the seasonal asymmetry and the spatial heterogeneity of the warming trend were less than those of $T_{s\text{-}max}$.

For $T_{s\text{-}min}$ and $T_{a\text{-}min}$, the warming rates were highest in North China and generally decreased from north to south (Figs. 4d and 4j). The average warming rates of $T_{s\text{-}min}$ and $T_{a\text{-}min}$ in the cold seasons (Figs. 4f and 4l) were faster than those in the warm seasons (Figs. 4e and 4k). This variation of warming rate with latitudes have been attributed to dynamics amplification (Wallace et al., 2012; Ding et al., 2014). In this study, we focus on the spatial heterogeneity of the warming rates at similar latitudes and diurnal contrast of the warming rates.

By contrasting the annual variation and spatial pattern of trends, we found that $T_s$ and $T_a$ had an extremely significant correlation with each other. Based on the time series

Atmos. Chem. Phys. Discuss., doi:10.5194/acp-2016-1022, 2016
Manuscript under review for journal Atmos. Chem. Phys.
Published: 19 December 2016


Atmospheric Chemistry and Physics Discussions

of national mean yearly anomalies (see Figs. 2 and Figs. 3), the correlations between $T_{s\text{-}max}$ and $T_{a\text{-}max}$ were 0.877, 0.799, and 0.921 on the annual, warm, and cold seasonal scales, respectively. The correlations between $T_{s\text{-}min}$ and $T_{a\text{-}min}$ were 0.976, 0.969, and 0.977 on the annual, warm, and cold seasonal scales, respectively. In the spatial pattern of the trends (Figs. 4), the correlations between $T_{s\text{-}max}$ and $T_{a\text{-}max}$ were 0.488, 0.465, and 0.522 on the annual, warm, and cold seasonal scales, respectively. Those between $T_{s\text{-}min}$ and $T_{a\text{-}min}$ were 0.638, 0.670, and 0.594 on the annual, warm, and cold seasonal scales, respectively.

In summary, $T_s$ had a significant correlation with Ta both in annual variation (Figs. 2 and Figs. 3) and in long-term trends (Figs. 4), indicating that $T_s$ observational records are reliable for climate change research. However, the correlation between $T_{s\text{-}min}$ and $T_{a\text{-}min}$ was significantly higher than that between $T_{s\text{-}max}$ and $T_{a\text{-}max}$. $T_{s\text{-}min}$ is closely related to the land–atmosphere longwave wave radiation balance during the nighttime, which is closely related to the atmospheric greenhouse effect (Dai et al., 1999). During the daytime, $T_s$ is directly determined by the land surface energy balance, i.e., the incoming energy including SSR and atmospheric longwave radiation (Wang and Dickinson, 2013a), and its partitions into latent and sensible heat fluxes (Zhou and Wang, 2016). Despite its dependence on the land-atmosphere sensible heat flux, $T_a$ is also impacted by local and/or large-scale circulation. So, the changes of land surface

Atmos. Chem. Phys. Discuss., doi:10.5194/acp-2016-1022, 2016
Manuscript under review for journal Atmos. Chem. Phys.
Published: 19 December 2016


Atmospheric Chemistry and Physics Discussions

energy balance caused by SSR and precipitation have different levels of effect on $T_s$ and $T_a$ during the day, which most likely causes a lower correlation between $T_{s\text{-}max}$ and $T_{a\text{-}max}$ than that between $T_{s\text{-}min}$ and $T_{a\text{-}min}$.

### 3.2. The impact of surface solar radiation and precipitation on temperatures

#### 3.2.1 Impact of surface solar radiation

Figs. S4 shows that SSR had an important relationship with $T_{s\text{-}max}$ and $T_{a\text{-}max}$ but not with $T_{s\text{-}min}$ and $T_{a\text{-}min}$. The national mean of the partial correlation coefficients between SSR and $T_{s\text{-}max}$ is 0.552 and 98.9% of the stations are statistically significant at the 1% level. Meanwhile, the national mean of the partial correlation coefficients between SSR and $T_{a\text{-}max}$ is 0.441, and 95.4% of the stations are statistically significant at the 1% level. This relationship is stronger in South China and on the North China Plain, i.e., it reaches 0.810 for $T_{s\text{-}max}$ and 0.765 for $T_{a\text{-}max}$.

$T_{s\text{-}max}$ is primarily determined by the land surface energy budget, whereas $T_{a\text{-}max}$ is influenced by the land surface energy flux and other factors, including both large-scale circulation and anthropogenic heat flux. Therefore, the correlation between $T_{s\text{-}max}$ and SSR is higher than that between $T_{a\text{-}max}$ and SSR (Figs. S4a and Figs. S4g). On the seasonal scales, the partial correlation between $T_{s\text{-}max}$ ($T_{a\text{-}max}$) and SSR in warm seasons

Atmos. Chem. Phys. Discuss., doi:10.5194/acp-2016-1022, 2016
Manuscript under review for journal Atmos. Chem. Phys.
Published: 19 December 2016


Atmospheric Chemistry and Physics Discussions

374 is higher than that in cold seasons, and the national mean partial correlation coefficients
375 for the warm and cold seasons are 0.579 and 0.498 for $T_{s\text{-}max}$ and 0.544 and 0.386 for
376 $T_{a\text{-}max}$, respectively, consisting with the seasonal cycle of SSR intensity over China.

377 Spatially, overall, the partial correlation coefficients between $T_{s\text{-}max}$ and $T_{a\text{-}max}$ and
378 SSR are higher in South China than in North China (see Figs. S4a–c and Figs. S4g–i).
379 South of 35° N, the national mean of the partial correlation coefficients between $T_{s\text{-}max}$
380 ($T_{a\text{-}max}$) and SSR is 0.654 (0.552), whereas that between $T_{s\text{-}max}$ ($T_{a\text{-}max}$) and SSR is just
381 0.417 in north of 35° N. During daytime, $T_s$ and $T_a$ is largely determined by how much
382 energy is used to evapotranspiration (Shen et al., 2014). In south China where soil
383 moisture is high, the energy used for evapotranspiration is near linearly related to SSR
384 (Wang and Dickinson, 2013b; Zhou et al., 2007). However, energy used for
385 evapotranspiration is more dependent on precipitation in the northwest China where the
386 soil is dry during most time of a year. As a result, the energy available for heating
387 surface and air temperature is not so closely related SSR. Therefore, the correlation
388 coefficients between SST and $T_{s\text{-}max}$ (or $T_{a\text{-}max}$) were stronger in south China. The
389 correlation between $T_{a\text{-}max}$ and SSR along the coast was significantly lower than inland
390 (see Figs. S4g-i), especially in the cold seasons (see Figs. S4i), probably because of the
391 stronger land-sea thermal convection along the coast.

Atmos. Chem. Phys. Discuss., doi:10.5194/acp-2016-1022, 2016
Manuscript under review for journal Atmos. Chem. Phys.
Published: 19 December 2016


Atmospheric Chemistry and Physics Discussions

392 To quantify the impact of SSR on temperature, the sensitivity of temperatures to
393 changes in SSR has been calculated (Eq. (2)). As Figs. S5 shows, $T_{s\text{-}max}$ was the most
394 sensitive to SSR, followed by $T_{a\text{-}max}$, and their national means were 0.092 °C（W $m^{-2}$)$^{-1}$
395 and 0.035 °C（W $m^{-2}$)$^{-1}$, respectively. $T_{s\text{-}min}$ and $T_{a\text{-}min}$ were insignificantly sensitive to
396 SSR because they primarily depend on atmospheric longwave radiation during the
397 nighttime.

398 Based on the above analysis, we calculated the impact of changes in SSR on
399 temperature (see the Method Section). From 1960–2003, the national mean decreasing
400 rate of SSR was −1.502 W $m^{-2}$ 10$yr^{-1}$, as calculated from monthly anomalies at 1,977
401 stations, and the trend was significant in most regions over China (see Figs. S6). Our
402 results are considerably less than the global average dimming rate (−2.3 ~ −5.1 W $m^{-2}$
403 10$yr^{-1}$) between the 1960s and the 1990s (Gilgen et al., 1998; Liepert, 2002; Stanhill
404 and Cohen, 2001; Ohmura, 2006) and the national mean dimming rate across China
405 (−2.9 ~ −5.2 W $m^{-2}$ 10$yr^{-1}$) between the 1960s and the 2000s based on radiation station
406 observations (Che et al., 2005; Liang and Xia, 2005; Shi et al., 2008; Wang et al., 2015a).

407 As noted in data section, the sensitivity drifting and replacement of the instruments
408 used for the SSR observations results in a significant homogenization in stations
409 observation records (Wang, 2014; Wang et al., 2015a), which causes a great uncertainty

Atmos. Chem. Phys. Discuss., doi:10.5194/acp-2016-1022, 2016
Manuscript under review for journal Atmos. Chem. Phys.
Published: 19 December 2016




in trend estimation. Tang et al. (2011) used quality-controlled observational data from 72 stations and two radiation models based on 479 stations to determine both that the dimming rate over China is −2.1 ~ −2.3 W $m^{-2}$ $10yr^{-1}$ during 1961-2000 and that the SSR has been essentially unchanged since 2000; this finding is generally consistent with our results.

Due to the decreasing trend in SSR, the warming trend of $T_{s\text{-}max}$ and $T_{a\text{-}max}$ decreased by 0.139 °C $10yr^{-1}$ and 0.053 °C $10yr^{-1}$, respectively, in the national mean. Spatially, the decreasing rate of SSR in South China and the North China Plain was significantly higher than in other regions, especially in the warm seasons (Figs. 5b). Therefore, the cooling effect of decreasing SSR on $T_{s\text{-}max}$ and $T_{a\text{-}max}$ was more significant in South China and the China North Plain, resulting in significantly lower warming rates of $T_{s\text{-}max}$ and $T_{a\text{-}max}$ there than in other regions (see Figs. 4). The spatial consistency between decreasing SSR and the warming slowdown of $T_{s\text{-}max}$ ($T_{a\text{-}max}$) implies that variation in SSR is the primary reason for the spatial heterogeneity of the warming rate in $T_{s\text{-}max}$ ($T_{a\text{-}max}$).

### 3.2.2 Impact of Precipitation

Figs. S7a shows that there is a significant negative correlation between $T_{s\text{-}max}$ and precipitation; the national mean of the partial correlation coefficients is −0.323, and

Atmos. Chem. Phys. Discuss., doi:10.5194/acp-2016-1022, 2016
Manuscript under review for journal Atmos. Chem. Phys.
Published: 19 December 2016


Atmospheric Chemistry and Physics Discussions

99.3% of the stations are statistically significant at the 1% level. Seasonally, the correlation is stronger in the warm seasons (regional mean: −0.405) than in the cold seasons (regional mean: −0.276). In warm seasons, the correlation in North China (regional mean: −0.459) is clearly stronger than in South China (regional mean: −0.365). In cold seasons, the correlation is highest on the Southwestern Yunnan-Guizhou Plateau and in most regions of North China (regional mean: −0.305) (Figs. S7b and Figs. S7c), whereas it is relatively weak in Southeastern China, the Tibet Plateau, Dzungaria, the Tarim Basin, and some regions of Northeastern China (regional mean: −0.117). The correlations between $T_{a\text{-}max}$ and precipitation have similar spatial and seasonal patterns (Figs. S7g–i) too, and 35.4% of the stations are statistically significant at the 1% level; these are primarily concentrated in arid and semiarid regions of China (regional mean: −0.167) (Figs. S7e–f and Figs. S7j–l).

Precipitation has a negative relationship with temperature because precipitation can reduce temperatures by increasing surface evaporative cooling (Dai et al., 1997; Wang et al., 2006). The impact of precipitation on temperature is higher in the warm seasons over China, which is consistent with seasonal changes in the correlation between $T_{s\text{-}max}$ and $T_{a\text{-}max}$ and precipitation (see Figs. S7b–c and Figs. S7h–i).

The national mean sensitivities of $T_{s\text{-}max}$ and $T_{a\text{-}max}$ to precipitation were −0.321 °C

Atmos. Chem. Phys. Discuss., doi:10.5194/acp-2016-1022, 2016
Manuscript under review for journal Atmos. Chem. Phys.
Published: 19 December 2016


Atmospheric Chemistry and Physics Discussions

446 10 $mm^{-1}$ and −0.064 °C 10 $mm^{-1}$, respectively. As shown in Figs. S8, there were
447 apparent seasonal and spatial changes in the sensitivity of $T_{s\text{-}max}$ and $T_{a\text{-}max}$ to
448 precipitation (Figs. S8a–c and Figs. S8g–i). In warm seasons, these sensitivities were
449 highest in the Tibet Plateau, the Loess Plateau, the Inter Mongolia Plateau, Dzungaria,
450 and the Tarim Basin (Figs. S8b and Figs. S8h). In cold seasons, the distribution of
451 regions with high sensitivity extended to all of North China and Southwest China (Figs.
452 S8c and Figs. S8i). Overall, the sensitivities of $T_{s\text{-}max}$ ($T_{a\text{-}max}$) were significantly higher
453 in arid regions (dry seasons) than in humidity regions (rainy seasons) (Wang and
454 Dickinson, 2013b). In contrast, $T_{s\text{-}min}$ and $T_{a\text{-}min}$ were less sensitive to variations in the
455 precipitation.

456 As Figs. 6 shows, during 1960-2003, the trend in the precipitation over the 1977
457 stations had obvious spatial heterogeneities. China's precipitation during this period
458 showed a slight increasing trend with an increasing rate of 0.112 mm $10yr^{-1}$.
459 Precipitation in Northwestern China and Southeastern China experienced an increasing
460 trend, whereas precipitation in the North China Plain, the Sichuan Basin, and parts of
461 Northeastern China experienced a decreasing trend. However, the trend of precipitation
462 was insignificant in most regions (see Figs. S6). Variation in precipitation had
463 significant seasonal differences (see Figs. 6b and Figs. 6c). The seasonal and spatial
464 characteristics of these precipitation variations are consistent with those identified in

Atmos. Chem. Phys. Discuss., doi:10.5194/acp-2016-1022, 2016
Manuscript under review for journal Atmos. Chem. Phys.
Published: 19 December 2016




previous studies (Zhai et al., 2005; Wang et al., 2015b).

Therefore, for $T_{a\text{-}max}$ and $T_{s\text{-}max}$, the reduction in precipitation aggravated the warming trend in the North China Plain, Sichuan Basin, and parts of Northeastern China, whereas the increase in precipitation primarily slowed the warming trend in Northwestern China and on the Mongolian Plateau (Figs. 6d). On national average, the impact of increasing precipitation resulted in the warming trends of $T_{s\text{-}max}$ and $T_{a\text{-}max}$ being decreased by −0.007 °C $10yr^{-1}$ and −0.002 °C $10yr^{-1}$, respectively. However, compared to SSR, the impact of precipitation on $T_{s\text{-}max}$ was smaller by approximately an order of magnitude. For $T_{s\text{-}min}$ and $T_{a\text{-}min}$, the impact of changes in precipitation was insignificant.

### 3.3. Trends of surface and air temperature after adjusting for the effect of SSR and precipitation

Based on the above analysis of the impact of SSR and precipitation on temperatures, we found that the variation of SSR and precipitation had little effect on $T_{s\text{-}min}$ and $T_{a\text{-}min}$. Therefore, we only analyzed their impact on $T_{s\text{-}max}$ and $T_{a\text{-}max}$. After adjusting for the impact of SSR and precipitation (Figs. 7), the warming rates of $T_{s\text{-}max}$ and $T_{a\text{-}max}$ increased by 0.146 °C $10yr^{-1}$ (64.3%) and 0.055 °C $10yr^{-1}$ (33.0%), respectively.

Atmos. Chem. Phys. Discuss., doi:10.5194/acp-2016-1022, 2016
Manuscript under review for journal Atmos. Chem. Phys.
Published: 19 December 2016


Atmospheric Chemistry and Physics Discussions

After adjusting, the seasonal contrast warming rates of $T_{s\text{-}max}$ and $T_{a\text{-}max}$ decreased by 45.0% and 17.2%. The national mean warming rate of $T_{s\text{-}max}$ increased by 0.178 °C $10yr^{-1}$ (103.1%) in the warm seasons and 0.086 °C $10yr^{-1}$ (27.2%) in the cold seasons. For $T_{a\text{-}max}$, the warming rate increased by 0.069 °C $10yr^{-1}$ (76.4%) in the warm seasons and 0.034 °C $10yr^{-1}$ (11.7%) in the cold seasons.

After adjusting for the impact of SSR and precipitation, the difference in warming rates between $T_{a\text{-}max}$ and $T_{a\text{-}min}$ changed from 0.190 to 0.134 °C $10yr^{-1}$, a decrease of 29.1%, and the difference between $T_{s\text{-}max}$ and $T_{s\text{-}min}$ changed from 0.088 to 0.058 °C $10yr^{-1}$, a decrease of 33.0%.

More importantly, after adjusting for the impact of SSR and precipitation, the spatial coherence of the warming rates of $T_{s\text{-}max}$ and $T_{a\text{-}max}$ in South and North China clearly improved (Figs. 8). The regional difference between the North China Plain, South China, and other regions in China shrank significantly due to the increase in the warming rates in South China and the North China Plain. In addition, the warming trend of $T_{s\text{-}max}$ and $T_{a\text{-}max}$ became more statistical significant in North China Plain and South China (see Figs. S9).

To further prove this, we selected two regions in China for further investigation: R1 primarily includes the North China Plain and R2 primarily includes the Loess

Atmos. Chem. Phys. Discuss., doi:10.5194/acp-2016-1022, 2016
Manuscript under review for journal Atmos. Chem. Phys.
Published: 19 December 2016




Plateau, as shown in Figs. 9a. These regions share same latitudes. However, the SSR showed substantially contrasting trends in the two regions (see Figs. 9b). After adjusting for the impacts of SSR and precipitation, the annual trends of $T_{s\text{-}max}$ and $T_{a\text{-}max}$ in R1 increased by 0.304 and 0.118 °C $10yr^{-1}$, while those in R2 just increased by 0.025 and 0.016 °C $10yr^{-1}$. The difference in warming rates of $T_{s\text{-}max}$ and $T_{a\text{-}max}$ between R1 and R2 reduced significantly after adjusting (see Figs. 9d).

Meanwhile, in R1, the seasonal and diurnal difference in the warming rates of $T_{s\text{-}max}$ and $T_{a\text{-}max}$ decreased significantly. After adjusting, in R1, the difference in warming rates between warm seasons and cold seasons decreased by 68.7% for $T_{s\text{-}max}$ and decreased by 50.8% for $T_{a\text{-}max}$. The difference in warming rates between $T_{s\text{-}max}$ and $T_{s\text{-}min}$ decreased by 93.4% and that between $T_{a\text{-}max}$ and $T_{a\text{-}min}$ decreased by 59.6%. The seasonal and diurnal difference of temperatures in R2 had no significant changes after adjusting. All in all, the trends of R1 and R2 became more consistent with each other after adjusting the difference in SSR and precipitation between them (see Figs. 9d).

## 4. Conclusions and Discussion

In China, despite the general warming trends over the entire country, warming trends showed significant spatial and temporal heterogeneity. In this paper, we analyzed the spatial and temporal patterns of Ts and Ta from 1960 to 2003 and further analyzed

Atmos. Chem. Phys. Discuss., doi:10.5194/acp-2016-1022, 2016
Manuscript under review for journal Atmos. Chem. Phys.
Published: 19 December 2016


Atmospheric Chemistry and Physics Discussions

519 and quantified the impact of SSR and precipitation on the temperature. The main results
520 are as follows.

521 The national mean warming rates of $T_{s\text{-}max}$, $T_{s\text{-}min}$, $T_{a\text{-}max}$, and $T_{a\text{-}min}$ were 0.227,
522 0.315 °C $10yr^{-1}$, 0.167 °C $10yr^{-1}$, and 0.356 °C $10yr^{-1}$, respectively, from 1960 to 2003.
523 The warming rates of $T_{s\text{-}min}$ and $T_{a\text{-}min}$ were significantly greater than those of $T_{s\text{-}max}$ and
524 $T_{a\text{-}max}$ (see Figs. 2 and Figs. 3). Warming rates of $T_{s\text{-}max}$ and $T_{a\text{-}max}$ in South China and
525 on the North China Plain were significantly lower than other regions (see Figs. 4). The
526 spatial heterogeneity in the warm seasons was greater than in the cold seasons.

527 During the study period, SSR decreased by $-1.502$ W $m^{-2}$ $10yr^{-1}$ in China, with
528 higher dimming rates in South China and the North China Plain. Using partial
529 regression analysis, we found that SSR was the primary cause of the spatial pattern in
530 the warming rates of $T_{s\text{-}max}$ and $T_{a\text{-}max}$. After adjusting for the impact of SSR and
531 precipitation, the warming trend of $T_{s\text{-}max}$ increased by 0.146 °C $10yr^{-1}$ and that of $T_{a\text{-}max}$
532 increased by 0.055 °C $10yr^{-1}$. After adjustments, the trends of $T_{s\text{-}max}$, $T_{s\text{-}min}$, $T_{a\text{-}max}$,
533 and $T_{a\text{-}min}$ became 0.373 °C $10yr^{-1}$, 0.315 °C $10yr^{-1}$, 0.222 °C $10yr^{-1}$, and 0.356 °C
534 $10yr^{-1}$. The reduction of SSR resulted in the warming rates of $T_{s\text{-}max}$ and $T_{a\text{-}max}$
535 decreasing by 0.139 °C $10yr^{-1}$ and 0.053 °C $10yr^{-1}$, accounting for 95.0% and 95.8%,
536 respectively, of the total impact of SSR and precipitation.

Atmos. Chem. Phys. Discuss., doi:10.5194/acp-2016-1022, 2016
Manuscript under review for journal Atmos. Chem. Phys.
Published: 19 December 2016


Atmospheric Chemistry and Physics Discussions

In addition to SSR and precipitation, temperatures' warming rates may be affected by many other factors, such as land cover change, that have not been discussed in this study due to lack of data, i.e., land cover and land use (Liu et al., 2005; Zhang et al., 2016). After adjusting for the impact of SSR and precipitation changes, spatial differences in the warming trends clearly decreased; however, some regional differences remain. The warming rate of $T_{s\text{-}max}$ in the Sichuan Basin remained significantly lower than in other regions after adjusting for these impacts. In addition, the north-south difference in the warming rates of $T_{s\text{-}min}$ and $T_{a\text{-}min}$ cannot be explained by the impacts of SSR and precipitation. Further study is needed.

**Acknowledgements** This study was funded by the National Natural Science Foundation of China (41525018 and 91337111) and the National Basic Research Program of China (2012CB955302). The latest meteorological datasets, collected at approximately 2400 meteorological stations in China were obtained from the China Meteorological Administration (CMA, http://data.cma.gov.cn/data).

Atmos. Chem. Phys. Discuss., doi:10.5194/acp-2016-1022, 2016
Manuscript under review for journal Atmos. Chem. Phys.
Published: 19 December 2016


Atmospheric Chemistry and Physics Discussions

## References

Ait-Mesbah, S., Dufresne, J. L., Cheruy, F., and Hourdin, F.: The role of thermal inertia in the representation of mean and diurnal range of surface temperature in semiarid and arid regions, Geophys Res Lett, 42, 7572-7580, 10.1002/2015gl065553, 2015.

Bounoua, L., Collatz, G. J., Sellers, P. J., Randall, D. A., Dazlich, D. A., Los, S. O., Berry, J. A., Fung, I., Tucker, C. J., Field, C. B., and Jensen, T. G.: Interactions between vegetation and climate: Radiative and physiological effects of doubled atmospheric CO2, J Climate, 12, 309-324, 10.1175/1520-0442(1999)012<0309:ibvacr>2.0.co;2, 1999.

Boyles, R. P., and Raman, S.: Analysis of climate trends in North Carolina (1949-1998), Environ Int, 29, 263-275, 10.1016/s0160-4120(02)00185-x, 2003.

Campbell, G. G., and VonderHaar, T. H.: Comparison of surface temperature minimum and maximum and satellite measured cloudiness and radiation budget, J Geophys Res-Atmos, 102, 16639-16645, 10.1029/96jd02718, 1997.

Cao, L., Zhu, Y., Tang, G., Yuan, F., and Yan, Z.: Climatic warming in China according to a homogenized data set from 2419 stations, Int J Climatol, 36, 4384-4392, 10.1002/joc.4639, 2016.

Che, H. Z., Shi, G. Y., Zhang, X. Y., Arimoto, R., Zhao, J. Q., Xu, L., Wang, B., and Chen, Z. H.: Analysis of 40 years of solar radiation data from China, 1961-2000, Geophys Res Lett, 32, 10.1029/2004gl022322, 2005.

Chen, H. S., Ma, H. D., Li, X., and Sun, S. L.: Solar influences on spatial patterns of Eurasian winter temperature and atmospheric general circulation anomalies, J Geophys Res-Atmos, 120, 8642-8657, 10.1002/2015jd023415, 2015.

Cheng, Z., Wang, S., Fu, X., Watson, J. G., Jiang, J., Fu, Q., Chen, C., Xu, B., Yu, J., Chow, J. C., and Hao, J.: Impact of biomass burning on haze pollution in the Yangtze River delta, China: a case study in summer 2011, Atmos. Chem. Phys., 14, 4573-4585, 10.5194/acp-14-4573-2014, 2014.

Christy, J. R., Norris, W. B., and McNider, R. T.: Surface Temperature Variations in East Africa and Possible Causes, J Climate, 22, 3342-3356, 10.1175/2008jcli2726.1, 2009.



579 Dai, A., DelGenio, A. D., and Fung, I. Y.: Clouds, precipitation and temperature range, Nature,
580 386, 665-666, 10.1038/386665b0, 1997.

581 Dai, A., Trenberth, K. E., and Karl, T. R.: Effects of clouds, soil moisture, precipitation, and
582 water vapor on diurnal temperature range, J Climate, 12, 2451-2473, 10.1175/1520-
583 0442(1999)012<2451:eocsmp>2.0.co;2, 1999.

584 Ding, Q., Wallace, J. M., Battisti, D. S., Steig, E. J., Gallant, A. J. E., Kim, H.-J., and Geng, L.:
585 Tropical forcing of the recent rapid Arctic warming in northeastern Canada and Greenland,
586 Nature, 509, 209-+, 10.1038/nature13260, 2014.

587 Duan, A., and Xiao, Z.: Does the climate warming hiatus exist over the Tibetan Plateau?, Sci.
588 Rep, 5, 10.1038/srep13711, 2015.

589 Easterling, D. R., Horton, B., Jones, P. D., Peterson, T. C., Karl, T. R., Parker, D. E., Salinger,
590 M. J., Razuvayev, V., Plummer, N., Jamason, P., and Folland, C. K.: Maximum and
591 minimum temperature trends for the globe, Science, 277, 364-367,
592 10.1126/science.277.5324.364, 1997.

593 Falge, E., Reth, S., Bruggemann, N., Butterbach-Bahl, K., Goldberg, V., Oltchev, A., Schaaf,
594 S., Spindler, G., Stiller, B., Queck, R., Kostner, B., and Bernhofer, C.: Comparison of
595 surface energy exchange models with eddy flux data in forest and grassland ecosystems
596 of Germany, Ecol Model, 188, 174-216, 10.1016/j.ecolmodel.2005.01.057, 2005.

597 Gettelman, A., and Fu, Q.: Observed and simulated upper-tropospheric water vapor feedback,
598 J Climate, 21, 3282-3289, 10.1175/2007jcli2142.1, 2008.

599 Gilgen, H., Wild, M., and Ohmura, A.: Means and trends of shortwave irradiance at the surface
600 estimated from global energy balance archive data, J Climate, 11, 2042-2061,
601 10.1175/1520-0442-11.8.2042, 1998.

602 Hartmann, D. L., Ramanathan, V., Berroir, A., and Hunt, G. E.: Earth radiation budget data and
603 climate research, Rev Geophys, 24, 439-468, 10.1029/RG024i002p00439, 1986.

604 Hartmann, D. L., Tank, A. M. G. K., and Rusticucci, M.: Observation: Atmosphere and surface,
605 IPCC, 1533 pp, 10.1017/CBO09781107415324, 2013.

606 Hegerl, G. C., and Zwiers, F. W.: Climate change 2007: Understanding and attributing climate
607 change, Cambridge University Press, 1007 pp., 2007.



608 Hingray, B., Mezghani, A., and Buishand, T. A.: Development of probability distributions for
609 regional climate change from uncertain global mean warming and an uncertain scaling
610 relationship, Hydrol Earth Syst Sc, 11, 1097-1114, 2007.

611 Huang, J., Guan, X., and Ji, F.: Enhanced cold-season warming in semi-arid regions, Atmos.
612 Chem. Phys., 12, 5391-5398, 10.5194/acp-12-5391-2012, 2012.

613 Jones, P. D., and Moberg, A.: Hemispheric and large-scale surface air temperature variations:
614 An extensive revision and an update to 2001, J Climate, 16, 206-223, 10.1175/1520-
615 0442(2003)016<0206:halssa>2.0.co;2, 2003.

616 Kalnay, E., and Cai, M.: Impact of urbanization and land-use change on climate, Nature, 423,
617 528-531, 10.1038/nature01675, 2003.

618 Karl, T. R., Kukla, G., Razuvayev, V. N., Changery, M. J., Quayle, R. G., Heim, R. R.,
619 Easterling, D. R., and Fu, C. B.: Global warming - evidence for asymmetric diurnal
620 temperature-change, Geophys Res Lett, 18, 2253-2256, 10.1029/91gl02900, 1991.

621 Karl, T. R., Jones, P. D., Knight, R. W., Kukla, G., Plummer, N., Razuvayev, V., Gallo, K. P.,
622 Lindseay, J., Charlson, R. J., and Peterson, T. C.: Asymmetric trends of daily maximum
623 and minimum temperature, B Am Meteorol Soc, 74, 1007-1023, 10.1175/1520-
624 0477(1993)074<1007:anporg>2.0.co;2, 1993.

625 Karoly, D. J., and Stott, P. A.: Anthropogenic warming of central England temperature, Atmos.
626 Sci. Lett., 7, 81-85, 10.1002/asl.136, 2006.

627 Kukla, G., and Karl, T. R.: Nighttime warming and the greenhouse-effect, Environ Sci Technol,
628 27, 1468-1474, 10.1021/es00045a001, 1993.

629 Lauritsen, R. G., and Rogers, J. C.: US Diurnal Temperature Range Variability and Regional
630 Causal Mechanisms, 1901-2002, J Climate, 25, 7216-7231, 10.1175/jcli-d-11-00429.1,
631 2012.

632 Li, B. F., Chen, Y. N., and Shi, X.: Why does the temperature rise faster in the arid region of
633 northwest China?, J Geophys Res-Atmos, 117, 10.1029/2012jd017953, 2012.

634 Li, Q. X., Yang, S., Xu, W. H., Wang, X. L. L., Jones, P., Parker, D., Zhou, L. M., Feng, Y., and
635 Gao, Y.: China experiencing the recent warming hiatus, Geophys Res Lett, 42, 889-898,
636 10.1002/2014gl062773, 2015.

637 Liang, F., and Xia, X. A.: Long-term trends in solar radiation and the associated climatic factors
638 over China for 1961-2000, Ann Geophys, 23, 2425-2432, 2005.

639 Liepert, B. G.: Observed reductions of surface solar radiation at sites in the United States and
640 worldwide from 1961 to 1990, Geophys Res Lett, 29, 10.1029/2002gl014910, 2002.

641 Lim, Y. K., Cai, M., Kalnay, E., and Zhou, L. M.: Observational evidence of sensitivity of
642 surface climate changes to land types and urbanization, Geophys Res Lett, 32, 4,
643 10.1029/2005gl024267, 2005.

644 Liu, B. H., Xu, M., Henderson, M., Qi, Y., and Li, Y. Q.: Taking China's temperature: Daily
645 range, warming trends, and regional variations, 1955-2000, J Climate, 17, 4453-4462,
646 10.1175/3230.1, 2004.

647 Liu, J. Y., Liu, M. L., Tian, H. Q., Zhuang, D. F., Zhang, Z. X., Zhang, W., Tang, X. M., and
648 Deng, X. Z.: Spatial and temporal patterns of China's cropland during 1990-2000: An
649 analysis based on Landsat TM data, Remote Sens Environ, 98, 442-456,
650 10.1016/j.rse.2005.08.012, 2005.

651 Mahlstein, I., and Knutti, R.: Regional climate change patterns identified by cluster analysis,
652 Clim Dynam, 35, 587-600, 10.1007/s00382-009-0654-0, 2010.

653 Makowski, K., Jaeger, E. B., Chiacchio, M., Wild, M., Ewen, T., and Ohmura, A.: On the
654 relationship between diurnal temperature range and surface solar radiation in Europe, J
655 Geophys Res-Atmos, 114, 16, 10.1029/2008jd011104, 2009.

656 Manara, V., Beltrano, M. C., Brunetti, M., Maugeri, M., Sanchez-Lorenzo, A., Simolo, C., and
657 Sorrenti, S.: Sunshine duration variability and trends in Italy from homogenized
658 instrumental time series (1936-2013), J Geophys Res-Atmos, 120, 3622-3641,
659 10.1002/2014jd022560, 2015.

660 Mariotti, L., Coppola, E., Sylla, M. B., Giorgi, F., and Piani, C.: Regional climate model
661 simulation of projected 21st century climate change over an all-Africa domain:
662 Comparison analysis of nested and driving model results, J Geophys Res-Atmos, 116,
663 10.1029/2010jd015068, 2011.

664 Menon, S., Hansen, J., Nazarenko, L., and Luo, Y. F.: Climate effects of black carbon aerosols
665 in China and India, Science, 297, 2250-2253, 10.1126/science.1075159, 2002.



666 Ohmura, A.: Observed long-term variations of solar irradiance at the earth's surface, Space Sci
667 Rev, 125, 111-128, 10.1007/s11214-006-9050-9, 2006.

668 Peng, S. S., Piao, S. L., Zeng, Z. Z., Ciais, P., Zhou, L. M., Li, L. Z. X., Myneni, R. B., Yin, Y.,
669 and Zeng, H.: Afforestation in China cools local land surface temperature, P Natl Acad Sci
670 USA, 111, 2915-2919, 10.1073/pnas.1315126111, 2014.

671 Ren, G., Xu, M., Chu, Z., Guo, J., Li, Q., Liu, X., and Wang, Y.: Changes of Surface Air
672 Temperature in China During 1951-2004, Climatic and environmental research, 10, 717-
673 727, 2005.

674 Roy, I., and Haigh, J. D.: The influence of solar variability and the quasi-biennial oscillation on
675 lower atmospheric temperatures and sea level pressure, Atmos. Chem. Phys., 11, 11679-
676 11687, 10.5194/acp-11-11679-2011, 2011.

677 Sanchez-Lorenzo, A., and Wild, M.: Decadal variations in estimated surface solar radiation
678 over Switzerland since the late 19th century, Atmos. Chem. Phys., 12, 8635-8644,
679 10.5194/acp-12-8635-2012, 2012.

680 Seneviratne, S. I., Corti, T., Davin, E. L., Hirschi, M., Jaeger, E. B., Lehner, I., Orlowsky, B.,
681 and Teuling, A. J.: Investigating soil moisture-climate interactions in a changing climate:
682 A review, Earth-sci Rev, 99, 125-161, 10.1016/j.earscirev.2010.02.004, 2010.

683 Shen, D. J., and Varis, O.: Climate change in China, Ambio, 30, 381-383, 10.1639/0044-
684 7447(2001)030[0381:ccic]2.0.co;2, 2001.

685 Shen, M. G., Piao, S. L., Jeong, S. J., Zhou, L. M., Zeng, Z. Z., Ciais, P., Chen, D. L., Huang,
686 M. T., Jin, C. S., Li, L. Z. X., Li, Y., Myneni, R. B., Yang, K., Zhang, G. X., Zhang, Y. J.,
687 and Yao, T. D.: Evaporative cooling over the Tibetan Plateau induced by vegetation growth,
688 P Natl Acad Sci USA, 112, 9299-9304, 10.1073/pnas.1504418112, 2015.

689 Shen, X. J., Liu, B. H., Li, G. D., Wu, Z. F., Jin, Y. H., Yu, P. J., and Zhou, D. W.: Spatiotemporal
690 change of diurnal temperature range and its relationship with sunshine duration and
691 precipitation in China, J Geophys Res-Atmos, 119, 13163-13179, 10.1002/2014jd022326,
692 2014.

693 Shi, G. Y., Hayasaka, T., Ohmura, A., Chen, Z. H., Wang, B., Zhao, J. Q., Che, H. Z., and Xu,
694 L.: Data quality assessment and the long-term trend of ground solar radiation in China, J.
695 Appl. Meteorol. Clim., 47, 1006-1016, 10.1175/2007jamc1493.1, 2008.



696 Stanhill, G., and Cohen, S.: Global dimming: a review of the evidence for a widespread and
697 significant reduction in global radiation with discussion of its probable causes and possible
698 agricultural consequences, Agr Forest Meteorol, 107, 255-278, 10.1016/s0168-
699 1923(00)00241-0, 2001.

700 Sun, Y., Zhang, X. B., Ren, G. Y., Zwiers, F. W., and Hu, T.: Contribution of urbanization to
701 warming in China, Nature Climate Change, 6, 706-+, 10.1038/nclimate2956, 2016.

702 Tang, W. J., Yang, K., Qin, J., Cheng, C. C. K., and He, J.: Solar radiation trend across China
703 in recent decades: a revisit with quality-controlled data, Atmos. Chem. Phys., 11, 393-406,
704 10.5194/acp-11-393-2011, 2011.

705 Taylor, J. R., Randel, W. J., and Jensen, E. J.: Cirrus cloud-temperature interactions in the
706 tropical tropopause layer: a case study, Atmos. Chem. Phys., 11, 10085-10095,
707 10.5194/acp-11-10085-2011, 2011.

708 Tebaldi, C., Smith, R. L., Nychka, D., and Mearns, L. O.: Quantifying uncertainty in projections
709 of regional climate change: A Bayesian approach (vol 18, pg 1524, 2005), J Climate, 18,
710 3405-3405, 10.1175/JCLI9001.1a, 2005.

711 Vautard, R., Yiou, P., and van Oldenborgh, G. J.: Decline of fog, mist and haze in Europe over
712 the past 30 years, Nat Geosci, 2, 115-119, 10.1038/ngeo414, 2009.

713 Vose, R. S., Easterling, D. R., and Gleason, B.: Maximum and minimum temperature trends for
714 the globe: An update through 2004, Geophys Res Lett, 32, 10.1029/2005gl024379, 2005.

715 Wallace, J. M., Fu, Q., Smoliak, B. V., Lin, P., and Johanson, C. M.: Simulated versus observed
716 patterns of warming over the extratropical Northern Hemisphere continents during the
717 cold season, P Natl Acad Sci USA, 109, 14337-14342, 10.1073/pnas.1204875109, 2012.

718 Wang, K., and Dickinson, R. E.: Global atmospheric downward longwave radiation at the
719 surface from ground-based observations, satellite retrievals, and reanalyses, Rev Geophys,
720 51, 150-185, 10.1002/rog.20009, 2013a.

721 Wang, K., and Dickinson, R. E.: Contribution of solar radiation to decadal temperature
722 variability over land, P Natl Acad Sci USA, 110, 14877-14882, 10.1073/pnas.1311433110,
723 2013b.

724 Wang, K. C., Li, Z. Q., and Cribb, M.: Estimation of evaporative fraction from a combination

of day and night land surface temperatures and NDVI: A new method to determine the Priestley-Taylor parameter, Remote Sens Environ, 102, 293-305, 10.1016/j.rse.2006.02.007, 2006.

Wang, K. C., and Dickinson, R. E.: A review of global terrestrial evapotranspiration: Observation, modeling, climatology, and climatic variability, Rev Geophys, 50, 10.1029/2011rg000373, 2012.

Wang, K. C., Dickinson, R. E., Wild, M., and Liang, S.: Atmospheric impacts on climatic variability of surface incident solar radiation, Atmos. Chem. Phys., 12, 9581-9592, 10.5194/acp-12-9581-2012, 2012.

Wang, K. C.: Measurement Biases Explain Discrepancies between the Observed and Simulated Decadal Variability of Surface Incident Solar Radiation, Sci. Rep, 4, 10.1038/srep06144, 2014.

Wang, K. C., Ma, Q., Li, Z. J., and Wang, J. K.: Decadal variability of surface incident solar radiation over China: Observations, satellite retrievals, and reanalyses, J Geophys Res-Atmos, 120, 6500-6514, 10.1002/2015jd023420, 2015a.

Wang, K. C., and Zhou, C. L. E.: Regional Contrasts of the Warming Rate over Land Significantly Depend on the Calculation Methods of Mean Air Temperature, Sci. Rep, 5, 10.1038/srep12324, 2015.

Wang, X., Wang, K., and Su, L.: Contribution of Atmospheric Diffusion Conditions to the Recent Improvement in Air Quality in China, Sci. Rep, 6, 36404, 10.1038/srep36404, 2016.

Wang, Y. J., Chen, X. Y., and Yan, F.: Spatial and temporal variations of annual precipitation during 1960-2010 in China, Quatern Int, 380, 5-13, 10.1016/j.quaint.2014.12.047, 2015b.

Weng, Q. H., Lu, D. S., and Schubring, J.: Estimation of land surface temperature-vegetation abundance relationship for urban heat island studies, Remote Sens Environ, 89, 467-483, 10.1016/j.rse.2003.11.005, 2004.

Wild, M., Ohmura, A., and Makowski, K.: Impact of global dimming and brightening on global warming, Geophys Res Lett, 34, 10.1029/2006gl028031, 2007.

Wild, M.: Enlightening global dimming and brightening, B Am Meteorol Soc, 93, 27-37,



754 10.1175/bams-d-11-00074.1, 2012.

755 Xia, X.: A closer looking at dimming and brightening in China during 1961-2005, Ann Geophys,
756 28, 1121-1132, 10.5194/angeo-28-1121-2010, 2010.

757 Yang, K., Koike, T., and Ye, B. S.: Improving estimation of hourly, daily, and monthly solar
758 radiation by importing global data sets, Agr Forest Meteorol, 137, 43-55,
759 10.1016/j.agrformet.2006.02.001, 2006.

760 Yin, Z., Wang, H., and Chen, H.: Understanding Severe Winter Haze Pollution in the North-
761 Central North China Plain in 2014, Atmos. Chem. Phys., 2016, 1-27, 10.5194/acp-2016-
762 641, 2016.

763 You, Q. L., Min, J. Z., Jiao, Y., Sillanpaa, M., and Kang, S. C.: Observed trend of diurnal
764 temperature range in the Tibetan Plateau in recent decades, Int J Climatol, 36, 2633-2643,
765 10.1002/joc.4517, 2016.

766 Zhai, P. M., Zhang, X. B., Wan, H., and Pan, X. H.: Trends in total precipitation and frequency
767 of daily precipitation extremes over China, J Climate, 18, 1096-1108, 10.1175/jcli-3318.1,
768 2005.

769 Zhang, X., Sun, Y., Mao, W., Liu, Y., and Ren, Y.: Regional Response of Temperature Change
770 in the Arid Regions of China to Global Warming, Arid Zone Research, 27, 592-599, 2010.

771 Zhang, Z. X., Li, N., Wang, X., Liu, F., and Yang, L. P.: A Comparative Study of Urban
772 Expansion in Beijing, Tianjin and Tangshan from the 1970s to 2013, Remote. Sen., 8, 22,
773 10.3390/rs8060496, 2016.

774 Zhou, C. L., and Wang, K. C.: Coldest Temperature Extreme Monotonically Increased and
775 Hottest Extreme Oscillated over Northern Hemisphere Land during Last 114 Years, Sci.
776 Rep, 6, 10.1038/srep25721, 2016.

777 Zhou, L. M., Dickinson, R. E., Tian, Y. H., Fang, J. Y., Li, Q. X., Kaufmann, R. K., Tucker, C.
778 J., and Myneni, R. B.: Evidence for a significant urbanization effect on climate in China,
779 P Natl Acad Sci USA, 101, 9540-9544, 10.1073/pnas.0400357101, 2004.

780 Zhou, L. M., Dickinson, R. E., Tian, Y. H., Vose, R. S., and Dai, Y. J.: Impact of vegetation
781 removal and soil aridation on diurnal temperature range in a semiarid region: Application
782 to the Sahel, P Natl Acad Sci USA, 104, 17937-17942, 10.1073/pnas.0700290104, 2007.



783 Zhou, L. M., Dai, A., Dai, Y. J., Vose, R., Zou, C. Z., Tian, Y. H., and Chen, H. S.: Spatial
784 dependence of diurnal temperature range trends on precipitation from 1950 to 2004, Clim
785 Dynam, 32, 429-440, 10.1007/s00382-008-0387-5, 2009.

786 Zhou, L. M., Dickinson, R. E., Dai, A. G., and Dirmeyer, P.: Detection and attribution of
787 anthropogenic forcing to diurnal temperature range changes from 1950 to 1999:
788 comparing multi-model simulations with observations, Clim Dynam, 35, 1289-1307,
789 10.1007/s00382-009-0644-2, 2010.

790 Zhou, Y. Q., and Ren, G. Y.: Change in extreme temperature event frequency over mainland
791 China, 1961-2008, Climate Res, 50, 125-139, 10.3354/cr01053, 2011.

792

793

794

795

796

797

798

Atmos. Chem. Phys. Discuss., doi:10.5194/acp-2016-1022, 2016
Manuscript under review for journal Atmos. Chem. Phys.
Published: 19 December 2016


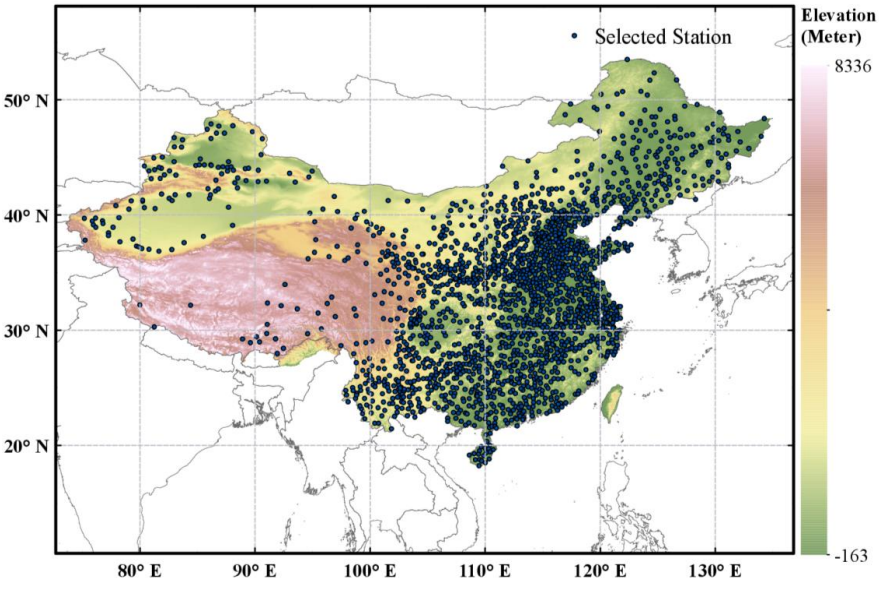


Figure. 1. Elevation maps of Mainland China and the spatial distribution of the 1977 meteorological stations used in this study. The datasets are provided by China's National Meteorological Information Center (You et al., 2016) (**http://data.cma.gov.cn/data**).

Atmos. Chem. Phys. Discuss., doi:10.5194/acp-2016-1022, 2016
Manuscript under review for journal Atmos. Chem. Phys.
Published: 19 December 2016


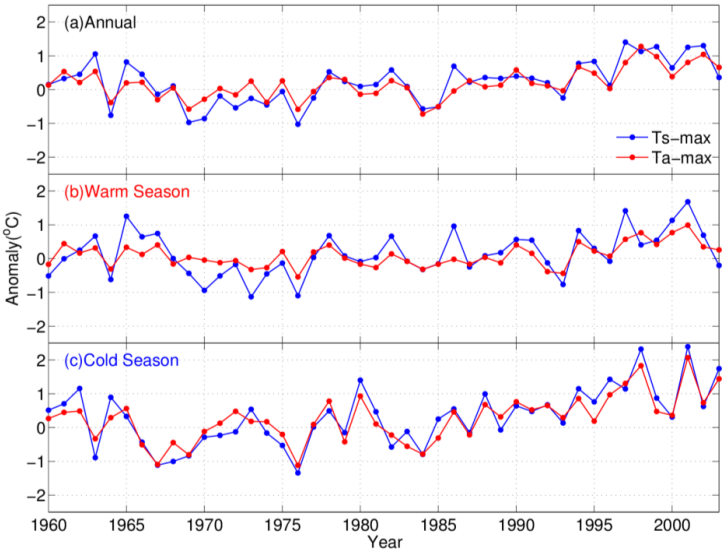


805

806 Figs. 2. National mean yearly anomalies of $T_{s\text{-}max}$ (blue line) and $T_{a\text{-}max}$ (red line) on

807 annual (a), warm (b), and cold (c) seasonal scales for the reference period of 1961–

808 1990.

Atmos. Chem. Phys. Discuss., doi:10.5194/acp-2016-1022, 2016
Manuscript under review for journal Atmos. Chem. Phys.
Published: 19 December 2016


Atmospheric Chemistry and Physics Discussions

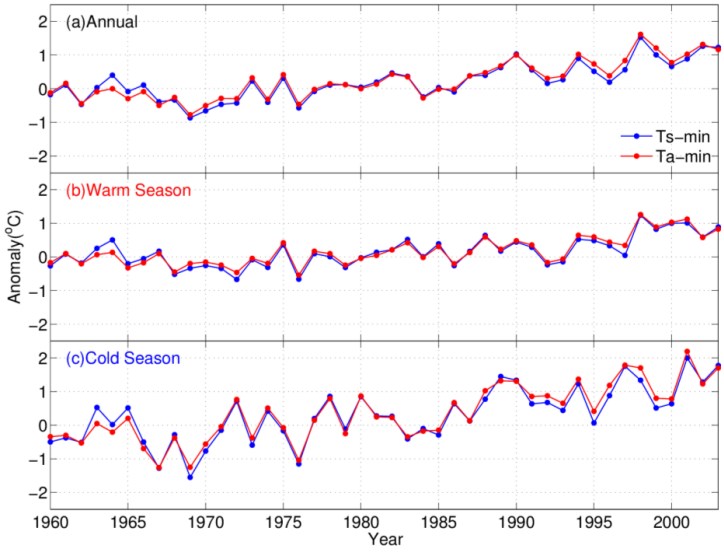


809

810 Figs. 3. National mean anomalies of $T_{s\text{-}min}$ (blue line) and $T_{a\text{-}min}$ (red line) on annual (a),

811 warm (b), and cold (c) seasonal scales for the reference period 1961-1990.

Atmos. Chem. Phys. Discuss., doi:10.5194/acp-2016-1022, 2016
Manuscript under review for journal Atmos. Chem. Phys.
Published: 19 December 2016


Atmospheric Chemistry and Physics Discussions

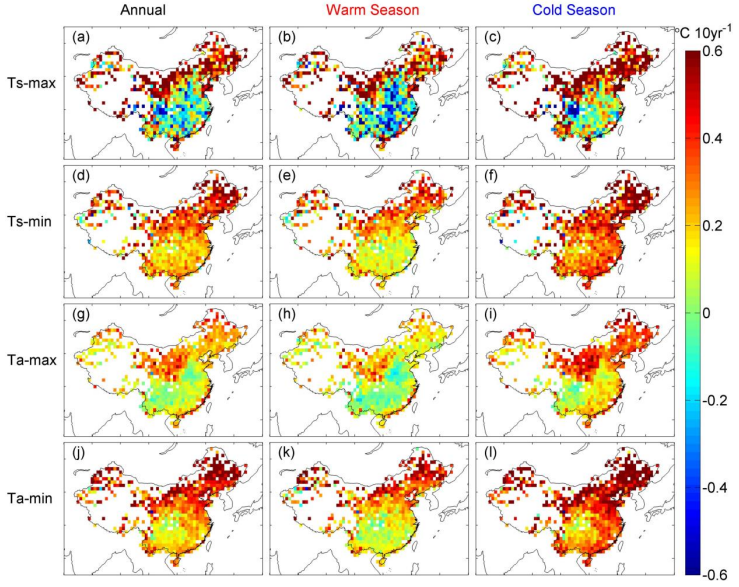


812

813 Figs. 4. Maps of the trends of the monthly anomalies for $T_{s\text{-}max}$ (a–c), $T_{s\text{-}min}$ (d–f), $T_{a\text{-}max}$

814 (g–i), and $T_{a\text{-}min}$ (j–l) on annual, warm (May–October), and cold (November–next April)

815 seasonal scales.

816

Atmos. Chem. Phys. Discuss., doi:10.5194/acp-2016-1022, 2016
Manuscript under review for journal Atmos. Chem. Phys.
Published: 19 December 2016


Atmospheric Chemistry and Physics Discussions

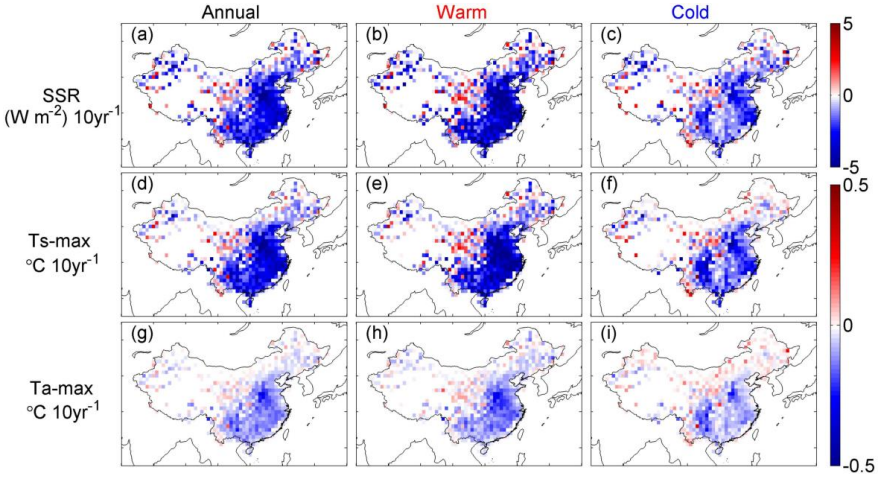


817

818 Figs. 5. Maps of the trends in surface solar radiation (SSR) (a–c) and its impact on the

819 warming rates of $T_{s\text{-}max}$ (d–f) and $T_{a\text{-}max}$ (g–i).

820

821

Atmos. Chem. Phys. Discuss., doi:10.5194/acp-2016-1022, 2016
Manuscript under review for journal Atmos. Chem. Phys.
Published: 19 December 2016




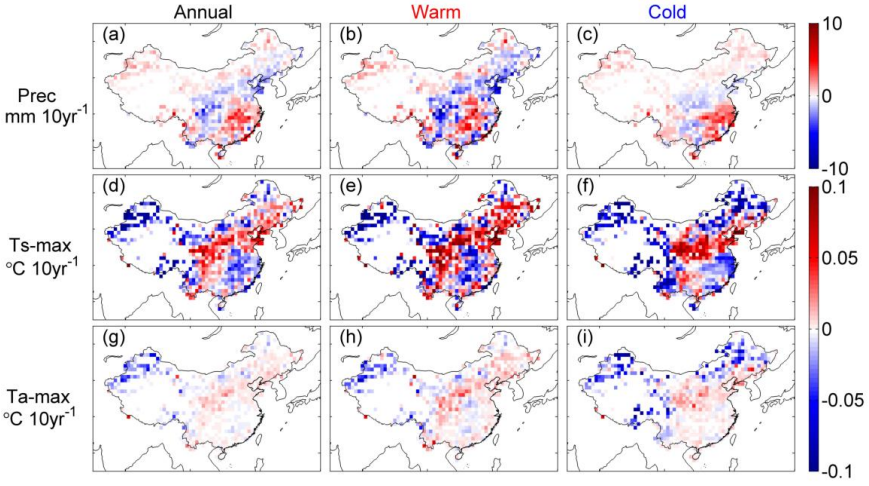


822

823 Figs. 6. Maps of the trends in precipitation (Prec) (a–c) and their impact on the warming

824 rates for $T_{s\text{-}max}$ (d–f) and $T_{a\text{-}max}$ (g–i).

825

826

Atmos. Chem. Phys. Discuss., doi:10.5194/acp-2016-1022, 2016
Manuscript under review for journal Atmos. Chem. Phys.
Published: 19 December 2016


Atmospheric Chemistry and Physics Discussions

827

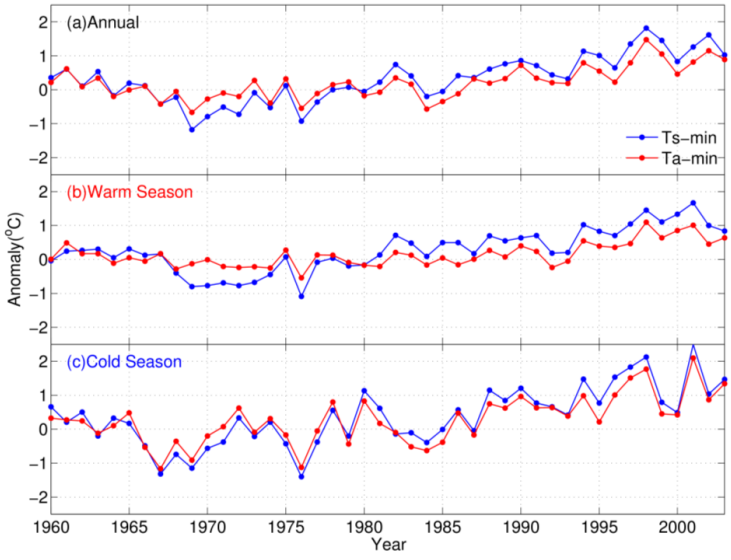


828 Figs. 7. After adjusting for the impact of SSR and precipitation, regionally average

829 anomalies of $T_{s\text{-}max}$ (blue line) and $T_{a\text{-}max}$ (red line) on annual (a), warm (b), and cold (c)

830 seasonal scales for the reference period of 1961-1990.

Atmos. Chem. Phys. Discuss., doi:10.5194/acp-2016-1022, 2016
Manuscript under review for journal Atmos. Chem. Phys.
Published: 19 December 2016


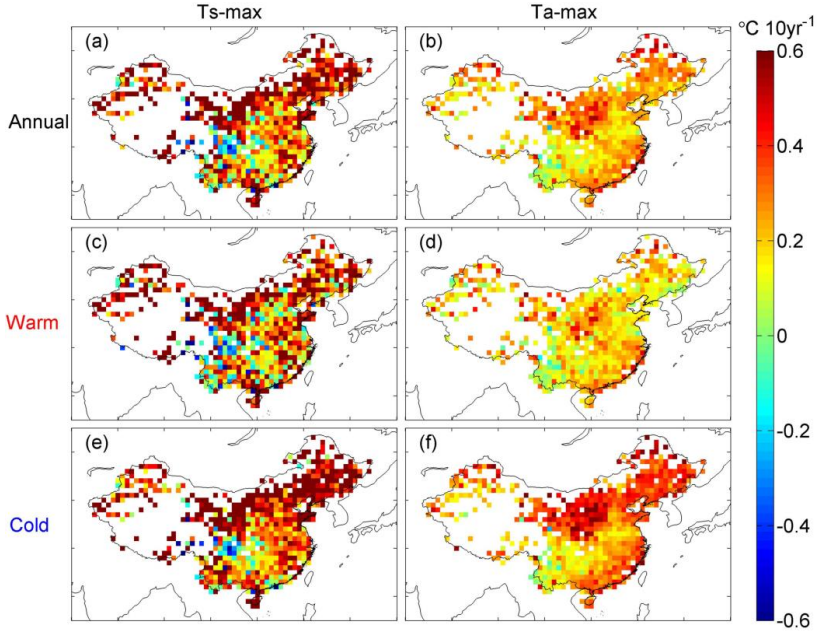


Figs. 8. After correcting for the impact of solar radiation and precipitation, maps of the trends of the monthly anomalies for $T_{s\text{-}max}$ (a, c, e) and $T_{a\text{-}max}$ (b, d, f) on the annual, warm, and cold seasonal scales.

Atmos. Chem. Phys. Discuss., doi:10.5194/acp-2016-1022, 2016
Manuscript under review for journal Atmos. Chem. Phys.
Published: 19 December 2016


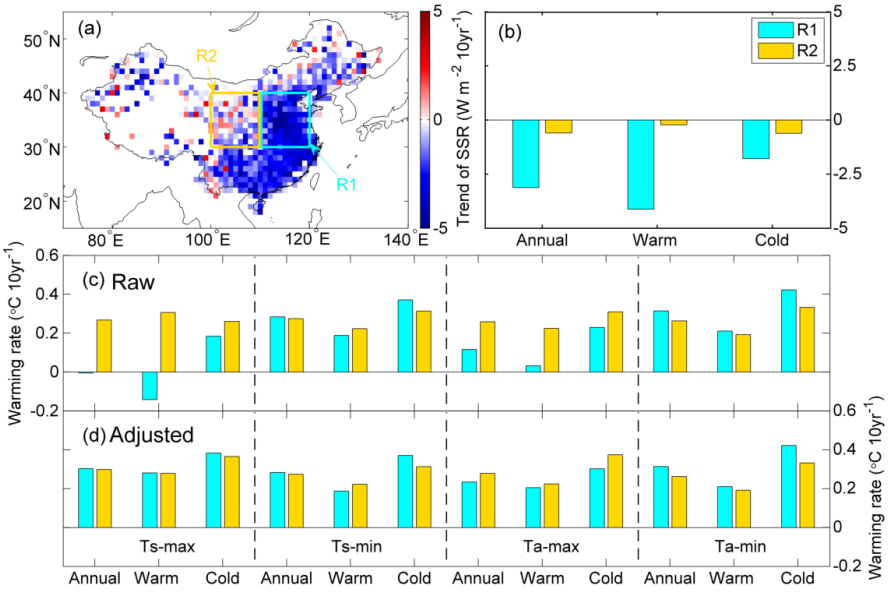


Figs. 9. (a) Maps of the trends of the surface solar radiation (SSR) and the location of the selected regions, R1 (latitude: 30° N–40° N; longitude: 110° N–120° N) and R2 (latitude: 30° N–40° N; longitude: 100° N–110° N). (b) The national mean trends of R1 and R2. (c) The trends on the annual, warm, and cold seasonal scales calculated based on the raw data (Raw). (d) The trends on the annual, warm, and cold seasonal scales calculated based on the adjusted data (Wang et al., 2015a), which does not include the impact of the surface solar radiation variation.

Atmos. Chem. Phys. Discuss., doi:10.5194/acp-2016-1022, 2016
Manuscript under review for journal Atmos. Chem. Phys.
Published: 19 December 2016


Atmospheric Chemistry and Physics Discussions

Table 1. The warming rates (units: °C 10yr$^{-1}$) of the temperatures on annual, warm, and cold seasonal scales. Raw and Adjusted represent the warming rates calculated for the data before and after adjusting for the impact of solar radiation and precipitation. Method I represents the first method, which calculates the national mean anomalies first and then calculates the national mean trend based on this time series; Method II represents second method, which calculates the trend of every grids first and then calculates the national mean value of the trends of all grids using the area-weight average method. We calculated the national mean trends of the temperatures using both methods.

| | | | $T_{s\text{-}max}$ | $T_{s\text{-}min}$ | $T_{a\text{-}max}$ | $T_{a\text{-}min}$ |
|---|---|---|---|---|---|---|
| Method I | Raw | Annual | 0.227 | 0.315 | 0.167 | 0.356 |
| | | Warm | 0.172 | 0.221 | 0.091 | 0.245 |
| | | Cold | 0.354 | 0.447 | 0.294 | 0.505 |
| | Adjusted | Annual | 0.373 | - | 0.222 | - |
| | | Warm | 0.350 | - | 0.160 | - |
| | | Cold | 0.450 | - | 0.329 | - |
| Method II | Raw | Annual | 0.254 | 0.328 | 0.183 | 0.368 |
| | | Warm | 0.193 | 0.235 | 0.104 | 0.256 |
| | | Cold | 0.321 | 0.415 | 0.264 | 0.476 |
| | Adjusted | Annual | 0.401 | - | 0.239 | - |
| | | Warm | 0.374 | - | 0.174 | - |
| | | Cold | 0.432 | - | 0.304 | - |